**1. Grzegorz KŁOSOWSKI[3], 2. Michał MAJ[1], 3. Michał OLESZEK[2]**

University of Economics and Innovation in Lublin (1), Research and Development Center Netrix S.A. (2), Lublin University of Technology (3)

1. 0000-0001-7927-3674, 2. 0000-0002-7604-8559 3. 0000-0002-8979-9650

doi:10.15199/48.2023.01.46

# Comparison of CNN and LSTM algorithms for solving the EIT inverse problem

***Abstract**. This article presents comparative research to verify the suitability of selected machine learning methods for the problem of solving the inverse problem in electrical impedance tomography. The research involved the use of a tomograph to image areas of moisture inside the walls. The measurement data collected by the tomograph was transformed into 3D spatial images using two types of artificial neural networks - convolutional neural network (CNN) and recurrent long short-term memory network (LSTM).*

***Streszczenie.** W tym artykule przedstawiono badania porównawcze w celu weryfikacji przydatności wybranych metod uczenia maszynowego do zagadnienia polegającego na rozwiązaniu problemu odwrotnego w elektrycznej tomografii impedancyjnej. Badania polegały na wykorzystaniu tomografu do obrazowania obszarów zawilgocenia wewnątrz murów. Zgromadzone za pomocą tomografu dane pomiarowe zostały przekształcone na obrazy przestrzenne 3D za pomocą dwóch rodzajów sztucznych sieci neuronowych – konwolucyjne sieci neuronowej (CNN) oraz sieci rekurencyjnej typu long short-term memory (LSTM). (**Porównanie algorytmów CNN i LSTM do rozwiązania problemu odwrotnego EIT**).*

**Keywords:** electrical tomography; machine learning; moisture detection, neural networks
**Słowa kluczowe:** tomografia elektryczna; uczenie maszynowe; wykrywanie wilgoci, sieci neuronowe.

## Introduction

Tomography belongs to the field of non-destructive testing, which is the only one that enables imaging of internal sections of walls in order to monitor moisture [1]. It can be used to create both 2D cross-section images and 3D spatial reconstructions. Contrary to standard methods, which enable humidity measurements only in selected points of the wall [2], tomographic images show larger areas. Thanks to the appropriate color calibration in the images, it is possible to effectively emphasize areas with higher humidity against the background of the fragments with a lower level of humidity, which can be considered as the background. So, tomography is a relative method that is not used to accurately measure the percentage of water content in porous walls, but it is a method that can monitor the spatial and relative distribution of moisture. In this study, the Electrical Impedance Tomography (EIT) was used to measure the humidity of the brick walls of the building [3–5]. The effectiveness of the tomographic system depends on the efficiency of the system for converting measurements to images. This is called an inverse problem that can be solved with deterministic or machine learning methods.

Deterministic methods rely on the appropriate selection of coefficients in the mathematical model. Examples of deterministic methods are Level Set, Gauss-Newton or Total Variation [6]. With appropriate iterative transformations, data from real or simulation measurements can be used to train machine learning-based models. In recent years, along with the development of information technology, machine learning methods have become increasingly popular. These are algorithmic methods that require a large amount of training data. Typically, the disadvantage of their use is the high computational complexity, which is associated with a high demand for computing power [7-11]. The most popular machine learning methodsre artificial neural networks, SVM, logistic and linear regression, LARS and elastic net [12]. Artificial neural networks include, inter alia, classical networks, which include the multilayer perceptron, convolutional neural networks and recursive LSTM networks [13].

Tomography is the only known method of imaging areas of humidity inside walls. It is also a non-invasive, non-destructive method. Commonly used methods are limited in scope and frequently destructive. This paper is mostly about describing the algorithmic methods that improve the quality and resolution of a tomographic image [14,15].

The negative economic effects of damp buildings are related to the fact that they are degraded by water. The subject of identifying the dampness in the walls of buildings is therefore important both from the point of view of society as a whole and from the point of view of an individual person. The authors' own contribution is the confirmation that both types of neural networks (CNN and LSTM) work well for tomographically identifying areas of moisture inside building walls where there is water damage.

## Materials and Methods

Figure 1 shows the examined fragment of a wall of a historical building with a tomograph and electrodes applied to the wall. The tomograph with electrodes was entirely designed and manufactured in the research and development center of Netrix SA. It is a prototype unit.

Fig.1. The measuring station equipped with an electric tomograph and two metal strips with 16 electrodes each

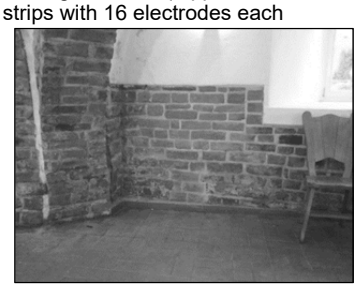

Fig.2. View of a fragment of the wall - a photo taken with an ordinary camera

Figures 2 and 3 show the same fragment of a building wall, but the photograph in Figure 1 was taken with an ordinary photosensitive camera. Figure 3 shows the same

wall as seen in infrared light. There are significant temperature differences in the range from 17.9 to 22 degrees Celsius.

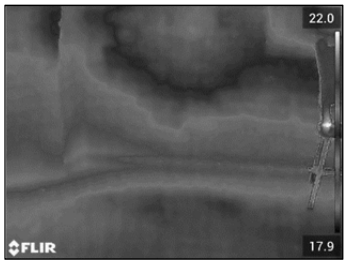


Fig. 3. View of a fragment of the wall - infrared photo

Damp surfaces evaporate more intensively, so their temperature is lower than that of dry surfaces. On this basis, it can be assumed that the lower the temperature, the more damp the wall surface is. The key word here is "surface". While infrared photography may serve as an approximate indicator of the moisture content of the external wall coatings, it does not answer the question about the distribution of moisture under their surface.

The tomograph used consisted of 32 electrodes arranged on two metal strips, each with 16 sensors. The electrodes are specially designed. Thanks to soft elements such as rubber and sponge, good contact is ensured on the uneven and porous surface of the brick wall. Care was also taken to minimize the contact resistance of the wall with the electrodes.

Using 32 electrodes made it possible to obtain 448 voltage measurements. Such a number of measurements is possible thanks to the multiplexer built into the tomograph, which switches the electric current source successively to individual electrodes and measures the voltage on a single electrode, which is also changed before each subsequent measurement. So, the whole measuring cycle is a set of measurements that are done in the right order. Therefore, since we are dealing with measurement cycles, the measurements within a given cycle form a measurement sequence consisting of 448 measurements, which in turn explains the use of the LSTM network. LSTM networks are great for making predictions about time series and data sequences because they can learn a lot from past trends.

The general model of the neural networks implemented can be written as $448 \rightarrow CNN \rightarrow 10752$ and $448 \rightarrow LSTM \rightarrow 10752$. The 3D output image is created on a mesh of 10752 tetrahedral finite elements. The measurement cases were generated using an algorithm that was created. It was necessary in order to obtain the appropriate number of observations to train the neural networks. The training set consisted of 30,000 observations. The algorithm solves a forward problem, i.e., on the basis of a randomly assigned moisture distribution in the tested fragment of the wall, the voltages between the individual pairs of electrodes are calculated. The research used the Eidors toolbox, which cooperates with the Matlab software [12].

Figure 4 shows the LSTM network architecture used in the research. LSTM networks are adapted to take into account many time steps, however in this case one measurement cycle constitutes one time step. This determines the appearance of Figure 4. Figure 5 shows the convolution method in the sequential (1D) layers of the CNN network. One value is created from a three-element filter. The main purpose of CNNs is to classify images. In this case, the regression problem is solved, and the input set is a vector, not an image.

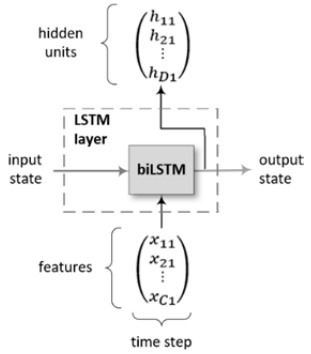


Fig. 4. The architecture of LSTM networks used

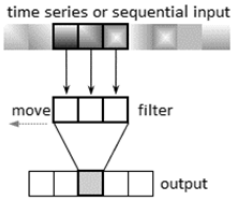


Fig. 5. Sequential layer convolution in CNN

Table 1 shows the seven layers of the CNN network. The first layer is sequential and contains 448 channels. The second layer is a weave and contains six 112-element filters. The third layer is ReLu, which zeros the negative values. The next layer is used to normalize the mini-batches. Layer 5 is global max pooling, which does downsampling by outputting the maximum time dimension of the input. The sixth layer is a fully connected layer, which in fact, acts as a multilayer perceptron with no transfer function, i.e., one which only sums up the products of weights and input values. The last layer is the regression layer that computes the half-mean-squared-error loss for regression tasks.

Table 1. Layers of the CNN network

| | Name | Activations | Learnable Properties |
|---|---|---|---|
| 1 | sequence<br>Sequence input with 448 dimensions | 448(C) × 1(B) × 1(T) | - |
| 2 | conv1d_1<br>112 4 convolutions with stride 1 and padding [4 4] | 112(C) × 1(B) × 6(T) | Weights 4 × 448 × 112<br>Bias 1 × 112 |
| 3 | relu_1<br>ReLU | 112(C) × 1(B) × 6(T) | - |
| 4 | batchnorm<br>Batch normalization | 112(C) × 1(B) × 6(T) | Offset 112 × 1<br>Scale 112 × 1 |
| 5 | gmpool1d<br>1-D global max pooling | 112(C) × 1(B) | - |
| 6 | fc_1<br>10752 fully connected layer | 10752(C) × 1(B) | Weights 10752 × 112<br>Bias 10752 × 1 |
| 7 | regressionoutput<br>mean-squared-error | 10752(C) × 1(B) | - |

Table 2 provides a description of the LSTM network layers. As with CNN, the first layer is sequential. It is aligned with a vector of 448 measured values. The second layer is a bidirectional LSTM with 2200 hidden units. The last two layers are the fully connected layer and the regression layer. The tasks of these layers are analogous to those of CNN.

Table 2. Layers of the LSTM network

| | Name | Activations | Learnable Properties |
|---|---|---|---|
| 1 | sequence<br>Sequence input with 448 dimensions | 448(C) × 1(B) × 1(T) | - |
| 2 | bilstm<br>BiLSTM with 2200 hidden units | 4400(C) × 1(B) | InputWeights 17600 × 448<br>RecurrentWeights 17600 × 2200<br>Bias 17600 × 1 |
| 3 | fc<br>10752 fully connected layer | 10752(C) × 1(B) | Weights 10752 × 4400<br>Bias 10752 × 1 |
| 4 | regressionoutput<br>mean-squared-error | 10752(C) × 1(B) | - |

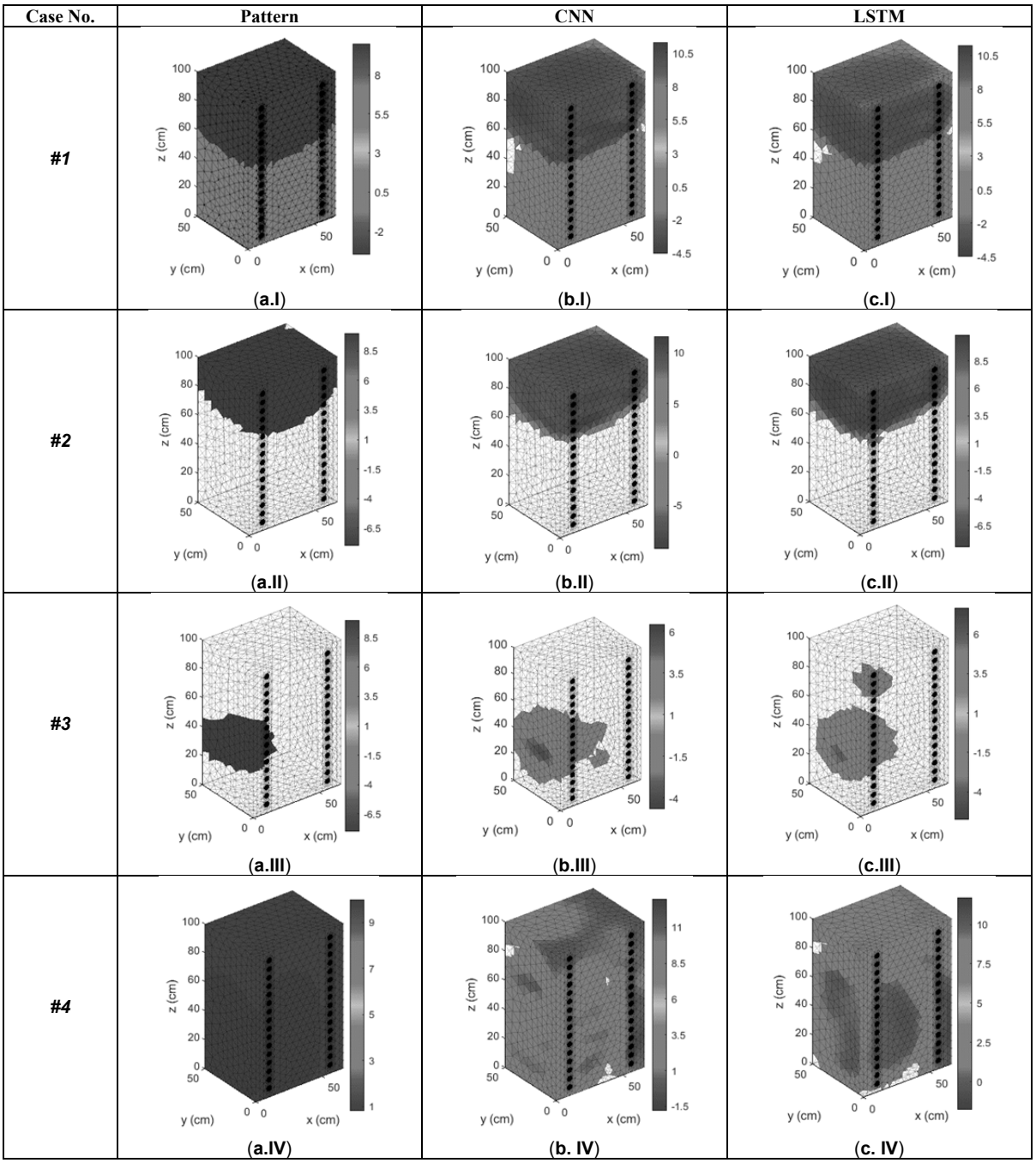


Fig. 7 Reconstructions obtained from simulation-generated measurements

The graphs in Figure 6 show the training performance of CNN and LSTM networks. The regular shape of the hyperbola and the lack of fluctuations show that the learning process is going in the right direction and give us a strong reason to believe that there is no overfitting.

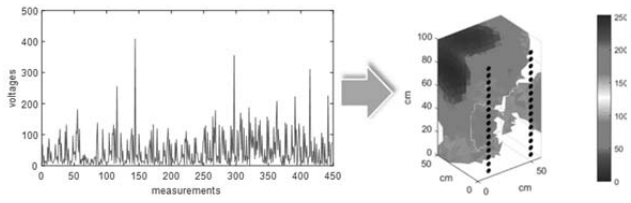


Fig.8. Tomographic distribution of moisture inside the wall generated by the CNN network based on the real measurement

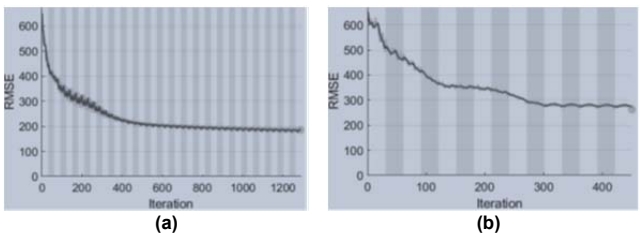


Fig.6. The training performance of neural networks: (a) – CNN, (b) - LSTM

The vertical axis shows the root mean square error (RMSE) values. The RMSE is calculated according to the formula (1)

(1) $$\mathrm{RMSE} = \sqrt{\frac{\sum_{i=1}^{n}(y_i - \hat{y}_i)^2}{n}}$$

where $y_i$ is the reference value of the *i*-th finite element of the reconstruction, $\hat{y}_i$ is the reconstruction value, and *n* is the total number of the image voxels (tetrahedrons).

**Results**

Figure 7 shows the comparative results of four selected four simulation test cases. The "Pattern" column contains reference images, while the next two columns contain reconstructions obtained using the CNN and LSTM methods, respectively. To increase the objectivity of the assessments, the reconstruction index analysis based on two quantitative criteria – the mean square error $\mathrm{MSE} = \sum_{i=1}^{n}(\Delta y_i)^2 / n$ and the image correlation coefficient (ICC) – was used. Formula (2) was used to calculate ICC metric

(2) $$\mathrm{ICC} = \frac{\sum_{i=1}^{n}(y_i - \bar{y})(\hat{y}_i - \bar{\hat{y}})}{\sqrt{\sum_{i=1}^{n}(y_i - \bar{y})^2 \sum_{i=1}^{n}(\hat{y}_i - \bar{\hat{y}})^2}}$$

where $y_i$ is the reference of the *i*-th voxel, $\hat{y}_i$ is the value of the reconstructed voxel, $\bar{y}$ is the mean reference distribution, and $\bar{\hat{y}}$ is the average distribution of the voxels reconstructed. The smaller the MSE is and the closer to 1 the ICC is, the better the reconstruction is. The results are presented in Table 3, which corresponds to Figure 7. The CNN method outperformed LSTM in cases II and III, while in cases I and IV the LSTM method turned out to be better.

Table 3. Indicators characterizing the quality of reconstructions for individual methods and observations.

| Observation | Indicator | Methods | |
|---|---|---|---|
| | | CNN | LSTM |
| I | MSE | 8.58 | 6.32 |
| | ICC | 0.89 | 0.9 |
| II | MSE | 3.33 | 4.69 |
| | ICC | 0.87 | 0.85 |
| III | MSE | 6.40 | 8.67 |
| | ICC | 0.83 | 0.79 |
| IV | MSE | 13.31 | 12.19 |
| | ICC | 0.77 | 0.78 |

Figure 8 shows an example of an EIT reconstruction based on actual measurements with the use of CNN. Due to the lack of a reference image, the correctness of the reconstruction cannot be verified. To do this, a direct method should be used (e.g., drying-weighing method), which, however, would injure the wall. Indirect point-by-point methods are less accurate (e.g., dielectric or microwave methods), so image validation was based on infrared images (see Figure 3).

**Conclusions**

The conducted comparative experiments have shown that both LSTM and CNN networks can be successfully used to convert measurements into images in EIT in the problem of moisture detection in building walls. Visual (subjective) observation of the images in Figure 7 confirms the results obtained with the use of quantitative (objective) indicators. Networks with simple architecture were used in the research. CNN contained only one convolution layer, and the LSTM network contained only one biLSTM layer. Despite this, it was quite easy to train effective machine learning-based models. In the future, research will focus on how to choose the best reconstruction techniques by taking into account different criteria and model parameters.

***Authors**: Grzegorz Kłosowski, Ph.D. Eng., Lublin University of Technology, Nadbystrzycka 38A, Lublin, Poland, E-mail: g.klosowski@pollub.pl; Michał Maj, M.Sc. Eng, University of Economics and Innovation, Projektowa 4, Lublin, Poland, E-mail: michal.maj@wsei.lublin.pl; Michał Oleszek, M.Sc. Eng., Netrix S.A., Research and Development Center, Związkowa 26, 20-148 Lublin, Poland, E-mail: michal.oleszek@netrix.com.pl*

REFERENCES

[1] Rymarczyk T., Kłosowski G., Hoła A., Hoła J., Sikora J., Tchórzewski P., Skowron Ł., Historical Buildings Dampness Analysis Using Electrical Tomography and Machine Learning Algorithms, Energies, 14 (2021), No. 5, 1307.
[2] Hoła, A. Methodology for the in Situ Testing of the Moisture Content of Brick Walls: An Example of Application. Archives of Civil and Mechanical Engineering, 20 (2020), No. 3, doi:10.1007/s43452-020-00120-3.
[3] Kłosowski G., Rymarczyk T., Kania K., Świć A., Cieplak T., Maintenance of industrial reactors supported by deep learning driven ultrasound tomography, Eksploatacja i Niezawodnosc – Maintenance and Reliability; 22 (2020), No 1, 138–147.
[4] Rymarczyk T., Niderla K. Kozłowski E. Król K., Wyrwisz J. Skrzypek-Ahmed S., Gołąbek P., Logistic Regression with Wave Preprocessing to Solve Inverse Problem in Industrial Tomography for Technological Process Control, Energies, 14 (2021), No. 23, 8116.
[5] Kania, W., Wajman, R., Ckript: a new scripting language for web applications, Informatyka, Automatyka, Pomiary W Gospodarce I Ochronie Środowiska, 12 (2022), No. 2, 4-9.
[6] Rymarczyk, T.; Kłosowski, G.; Hoła, A.; Sikora, J.; Wołowiec, T.; Tchórzewski, P.; Skowron, S. Comparison of Machine Learning Methods in Electrical Tomography for Detecting Moisture in Building Walls. Energies (Basel), 14 (2021), 2777, doi:10.3390/en14102777.
[7] Koulountzios P., Aghajanian S., Rymarczyk T., Koiranen T., Soleimani M., An Ultrasound Tomography Method for Monitoring CO2 Capture Process Involving Stirring and CaCO3 Precipitation, Sensors, 21 (2021), No. 21, 6995.
[8] Kania K., Rymarczyk T., Mazurek M., Skrzypek-Ahmed S., Guzik M., Oleszczuk P., Optimisation of Technological Processes by Solving Inverse Problem through Block-Wise-Transform-Reduction Method Using Open Architecture Sensor Platform, Energies, 14 (2021), No. 24, 8295.
[9] Styła, M., Adamkiewicz, P., Hybrid navigation system for indoor use. Informatyka, Automatyka, Pomiary W Gospodarce I Ochronie Środowiska, 12 (2022), No. 1, 10-14.
[10] Korzeniewska, E., Sekulska-Nalewajko, J., Gocawski, J., Drożdż, T., Kiebasa, P., Analysis of changes in fruit tissue after the pulsed electric field treatment using optical coherence tomography, EPJ Applied Physics, 91 (2020), No. 3, 30902.
[11] Korzeniewska, E., Krawczyk, A., Mróz, J., Wyszyńska, E., Zawiślak, R., Applications of smart textiles in post-stroke rehabilitation, Sensors (Switzerland), 20 (2020), No. 8, 2370.
[12] Rymarczyk, T.; Kozłowski, E.; Kłosowski, G. Electrical Impedance Tomography in 3D Flood Embankments Testing – Elastic Net Approach. Transactions of the Institute of Measurement and Control, 42 (2019), 680–690, doi:10.1177/0142331219857374.
[13] Fabijańska, A.; Banasiak, R. Graph Convolutional Networks for Enhanced Resolution 3D Electrical Capacitance Tomography Image Reconstruction. Appl Soft Comput, 110 (2021), 107608, doi:10.1016/J.ASOC.2021.107608.
[14] Tang, H.; Xu, C.; Han, X. Electrical Resistance Tomography Image Reconstruction Based on One-Dimensional Multi-Branch Convolutional Neural Network Combined with Attention Mechanism. Flow Measurement and Instrumentation, 84 (2022) , 102140, doi:10.1016/J.FLOWMEASINST.2022.102140.
[15] Dimas, C.; Sotiriadis, P.P. Electrical Impedance Tomography Image Reconstruction for Adjacent and Opposite Strategy Using FEMM and EIDORS Simulation Models. 2018 7th International Conference on Modern Circuits and Systems Technologies, MOCAST 2018, (2012) 1–4, doi:10.1109/MOCAST.2018.8376604.